## FULL PAPER

# Initial clinical observations of intra- and interfractional motion variation in MR-guided lung SBRT

[1]DAVID H THOMAS, PhD, [2]ANAND SANTHANAM, PhD, [2]AMAR U KISHAN, MD, [2]MINSONG CAO, PhD, [2]JAMES LAMB, PhD, [2]YUGANG MIN, PhD, [2]DYLAN O'CONNELL, MS, [2]YINGLI YANG, PhD, [2]NZHDE AGAZARYAN, PhD, [2]PERCY LEE, MD and [2]DANIEL LOW, PhD

[1]Department of Radiation Oncology, University of Colorado School of Medicine, Aurora, CO, USA
[2]Department of Radiation Oncology, University of California, Los Angeles, CA, USA

Address correspondence to: Mr David H Thomas
E-mail: *david.h.thomas@ucdenver.edu*

**Objective:** To evaluate variations in intra- and interfractional tumour motion, and the effect on internal target volume (ITV) contour accuracy, using deformable image registration of real-time two-dimensional-sagittal cine-mode MRI acquired during lung stereotactic body radiation therapy (SBRT) treatments.

**Methods:** Five lung tumour patients underwent free-breathing SBRT treatments on the ViewRay system, with dose prescribed to a planning target volume (defined as a 3–6 mm expansion of the 4DCT-ITV). Sagittal slice cine-MR images ($3.5 \times 3.5 \, mm^2$ pixels) were acquired through the centre of the tumour at 4 frames per second throughout the treatments (3–4 fractions of 21–32 min). Tumour gross tumour volumes (GTVs) were contoured on the first frame of the MR cine and tracked for the first 20 min of each treatment using offline optical-flow based deformable registration implemented on a GPU cluster. A ground truth ITV (MR-ITV$_{20 \, min}$) was formed by taking the union of tracked GTV contours. Pseudo-ITVs were generated from unions of the GTV contours tracked over 10 s segments of image data (MR-ITV$_{10 \, s}$).

**Results:** Differences were observed in the magnitude of median tumour displacement between days of treatments. MR-ITV$_{10 \, s}$ areas were as small as 46% of the MR-ITV$_{20 \, min}$.

**Conclusion:** An ITV offers a "snapshot" of breathing motion for the brief period of time the tumour is imaged on a specific day. Real-time MRI over prolonged periods of time and over multiple treatment fractions shows that ITV size varies. Further work is required to investigate the dosimetric effect of these results.

**Advances in knowledge:** Five lung tumour patients underwent free-breathing MRI-guided SBRT treatments, and their tumours tracked using deformable registration of cine-mode MRI. The results indicate that variability of both intra- and interfractional breathing amplitude should be taken into account during planning of lung radiotherapy.

## INTRODUCTION

Intra- and interfractional motion remains one of the biggest challenges in radiation therapy. In thoracic and abdominal sites, four-dimensional CT (4DCT) techniques that allow both the range of motion as well as the mean tumour position to be determined are regularly employed. Using respiratory gating, 4DCT methods assume that respiratory motion is approximately periodic, and that the depth of breathing can be assumed to remain constant from cycle-to-cycle with no interfractional variation. Respiratory-gated 4DCT techniques also enable the calculation of an averaged CT image or maximum intensity projection (MIP).[1] Often, the internal target volume (ITV) is the union of all tumour positions during the 4DCT.[2] For many patients, breathing patterns are stable and regular, with naturally repeated cycles that are reasonably periodic, but various studies have shown that irregularities in breathing patterns can lead to the ITV underestimating the true range of motion.[3,4]

The introduction of MRI-guided radiotherapy systems allows real-time soft-tissue imaging during delivery of radiotherapy. The only clinical system currently in use is the ViewRay® MRIdian, a commercially available MRI-guided Co-60 radiotherapy system that uses three Co-60 sources combined with a 0.35 T MRI system for patient setup and real-time tumour motion tracking during treatment. Real-time cine imaging is currently limited to two-dimensional (2D) sagittal planes.

MRI offers specific advantages for the real-time delineation of certain tumours owing to improved soft-tissue contrast, but image quality is generally degraded by motion.[5] Various

Table 1. Literature summary of studies evaluating MRI-based lung tumour motion

| Author | Year | Number of subjects | Frames per second | Session time (s) | Number of sessions |
|--------|------|-------------------|-------------------|------------------|--------------------|
| Koch[14] | 2004 | 7 (3 healthy volunteers, 4 lung cancer patients) | 2.2 | 45 | 2 |
| Lui[14] | 2004 | 7 (3 healthy volunteers, 4 lung cancer patients) | 2.2 | 45 | 2 |
| Plathow[15] | 2004 | 20 lung patients | 0.3 | 30 | 1 |
| Blackall[7] | 2006 | 10 volunteers, 5 lung cancer patients. | 3 | Several minutes | 1 |
| Cai[16] | 2007 | 3 healthy volunteers | 10 | 300 | 2 |
| Cai[16] | 2007 | 14 (8 healthy volunteers, 6 lung cancer patients) | 3 | 300 | 1 |
| Cai[12] | 2008 | 17 (9 healthy volunteers, 8 lung cancer patients) | 10 | 300 | 2 |
| Cai[13] | 2008 | 15 (7 healthy volunteers, 8 lung cancer patients) | 3 | 300 | 1 |
| Cai[3] | 2010 | 18 (10 healthy volunteers, 8 lung cancer patients) | 3 | 300 | 1 |
| Seregni[8] | 2016 | 6 lung cancer patients | 4 | 256 | 1 |
| Thomas[a] | 2016 | 5 lung cancer patients | 4 | 1200 | 3–4 |

[a]The current study is indicated.

studies have employed single-slice 2D dynamic MRI to measure respiratory motion. Several studies,[3,6–13] have all employed fast-sequence cine-mode MRI of free breathing patients to investigate the reproducibility of respiratory motion, but limitations of these studies include either short imaging sessions or only a single study session. Various imaging parameters and study size/durations are summarized in Table 1.

This study reports tumour tracking results from five lung tumour patients who underwent free-breathing stereotactic body radiation therapy (SBRT) treatment on the ViewRay MRIdian at the UCLA Department of Radiation Oncology. Lung tumours were tracked for 20 mins per fraction for 3 or 4 fractions of treatment, and the inter- and intrafractional motion analysed with regards to the variation in ITV margin.

**METHODS AND MATERIALS**
Five patients (three male, two female) were treated under free-breathing with lung SBRT on the ViewRay system. Patient ages were 59, 68, 69, 72, 73. Simulation took place on both CT, including 4DCT and MRI (ViewRay), on the same day. Free-breathing MRI scans of 172 s duration were acquired (Siemens TrueFISP; repetition time = 3.37 ms, echo time = 1.45 ms) with $1.5 \times 1.5 \times 1.5$ mm$^3$ resolution. Table 2 shows the tumour locations. Gross tumour volumes (GTVs) were contoured by a physician, and ITV's were contoured on both 4DCT and MRI. It was assumed that the 172 s free-breathing acquisitions captured sufficient motion, *i.e.* similar to the 4DCT, to be considered an ITV.

MRI-guided treatments were performed with real-time 2D cine-mode MR imaging performed using the 0.35 T whole body MRI scanner included with the ViewRay system. A balanced steady-state free precession sequence (Siemens TrueFISP; repetition time = 2.1 ms, echo time = 0.91 ms) was used to acquire images of a single 5 mm thick sagittal slice through the centre of the tumour at 4 fps, with a $35 \times 35$ cm$^2$ field of view with $3.5 \times 3.5$ mm$^2$ spatial resolution. Five patients received three to four fractions of treatment with cine-mode

imaging of duration greater than 20 min acquired each fraction. Patients with central lung tumours ($N = 2$) received 50 Gy in four fractions, and patients with peripheral lung tumours ($N = 3$) received 54 Gy in three fractions. Cine-mode images were exported from the ViewRay system after each treatment, and converted to DICOM (**Digital Imaging and Communications in Medicine**) format using Matlab® R2016 (The Math-Works, Inc., Natick, MA) and subsequently exported to MIM v. 6 (MIM Software, Cleveland, OH) for contouring. The GTV was contoured on the first cine frame of each fraction by a physician. Images were then exported to a graphics processing unit (GPU) cluster for deformable image registration (DIR) in order to propagate the GTV onto each frame of the cine. A well-validated anatomy-based multilevel multiresolution optical flow and thin-plate splines[17, 18] method was used. This method characterizes a three-dimensional (3D) object in 2D images as features and correlates the features from one image to another in such a way that the cumulative intensity displacement gradient is minimized. The optical flow registration method starts with an initial estimated displacement (typically set to zero for each voxel) and then refines it according to partial derivative of voxel intensity and weighted sum of displacement from all nearby voxels. Displacement estimation is iteratively updated until the displacement in the whole field converges.[19] One advantage of this method is that it tracks the overall motion of the field even if some feature points cannot be tracked, although this is not exclusive to this method. Each frame of the cine was registered to the first frame, and the subsequent deformation vectors used to warp the GTV contour. The accuracy of the DIR generated contours was checked visual in all images, and spot-checked in comparison to manually generated contours in 10 frames per fraction. For each time point $t$, the centroid of the GTV was recorded, as well as a cumulative ITV generated from the union of all GTVs from times time = 0 to time = $t$. Figure 1 shows a final cine frame with the GTV tracked across four fractions of treatment for Patient 1, with the ITV generated from the union of all GTV contours tracked for 20 min in each case (MR-ITV$_{20 min}$).

Table 2. Tumour size (GTV) and motion (ITV), and associated motion of GTV centroid as measured during simulation; data from 4DCT and free-breathing (172 s) MRI (bottom row)

| Simulation | Patient 1 Contour size (mm) | Patient 1 Motion (mm) | Patient 2 Contour size (mm) | Patient 2 Motion (mm) | Patient 3 Contour size (mm) | Patient 3 Motion (mm) | Patient 4 Contour size (mm) | Patient 4 Motion (mm) | Patient 5 Contour size (mm) | Patient 5 Motion (mm) |
|---|---|---|---|---|---|---|---|---|---|---|
| CT GTV[a] | 28.7 | – | 43.2 | – | 27 | – | 14.6 | – | 14.8 | – |
| 4DCT ITV[a] | 41.7 | 13 | 49.8 | 6.6 | 31.6 | 4.6 | 21.1 | 6.5 | 21.2 | 6.4 |
| FB MRI ITV[a] | 38.9 | 10.2 | 59.3 | 16.1 | 35.6 | 8.6 | 21.9 | 7.3 | 23.7 | 8.9 |
| Location | Right lower lung | | Right lower lung | | Right upper lung | | Right medial lung | | Right medial lung | |
| Cine mode | Mean motion (mm) | σ (mm) | Mean motion (mm) | σ (mm) | Mean motion (mm) | σ (mm) | Mean motion (mm) | σ (mm) | Mean motion (mm) | σ (mm) |
| Fraction 1 | 11.1 | 2.0 | 9.4 | 2.0 | 8.4 | 1.7 | 1.9 | 1.2 | | – |
| Fraction 2 | 13.7 | 1.3 | 11.0 | 2.2 | 3.0 | 1.2 | 3.5 | 0.9 | | |
| Fraction 3 | 18.0 | 3.0 | 6.0 | 0.8 | 4.8 | 1.5 | 2.0 | 0.4 | | |
| Fraction 4 | 15.2 | 3.3 | – | – | 5.1 | 1.1 | – | – | | |

[a]Measured along dimension of maximum motion, through the central slice

Cine mode measured motion (mean and standard deviation) of GTV centroid.

Figure 1. Example sagittal 2D cine-mode imaging during four fractions of treatment for Patient 1. GTV tracking from the off-line deformable image registration is shown for each fraction (inner contour), with the cumulative ITV for the entire fraction also plotted (outer contour). 2D, two-dimensional; GTV, gross tumour volume; ITV, internal target volume.
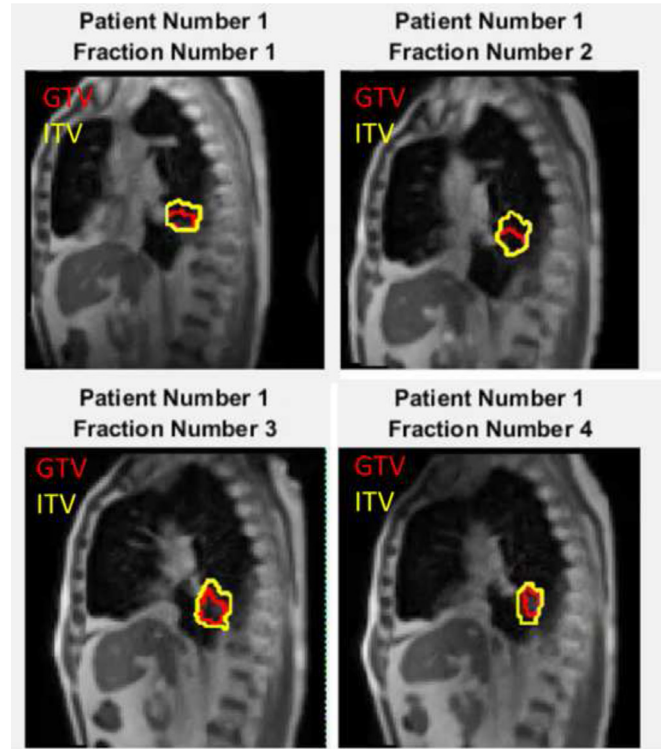


A breathing trace for each fraction was generated by calculating the vector displacement length of the GTV centroid from the 5th percentile of motion in the anterioposterior (AP) and craniocaudal (CC) directions. The time points at which local peaks of inhalation occurred were extracted from a version of the trace smoothed using a median filter, and the amplitude of each peak subsequently identified from the original data. The mean breathing period was determined from the mean duration between peaks, and any peak occurring less than an arbitrary threshold of 10% of the mean period, chosen from visual inspection of the data, was determined to be noise in the data and rejected from the analysis. The variation in the magnitude of tumour centroid displacement was analysed using the boxplot function in Matlab Statistics Toolbox (R2016).

A simulation was performed to determine the variation in the dimensions of ITV contours as although the patient had been scanned using a commercial low-pitch helical CT protocol and retrospective phase-based sorting technique. For this simulation, the scanner parameters were taken from the Phillips Big Bore 4DCT protocol: pitch of 0.06, rotation time of 0.5 s and detector width of 2.4 cm. This translated to an imaging time of approximately 10 s for stationary tissues. For each 1 s of the GTV tracking data per fraction, an ITV was generated from the union of the corresponding GTV contours from the following 10 s of image data (MR-ITV$_{10 s}$). The variation in the MR-ITV$_{10 s}$

Figure 2. GTV tracking data for Patient 1. (a) Shows AP *vs* CC motion of the GTV centroid for Patient 1, Fractions 1–4 (first 500 s of each fraction shown), showing interfractional variation in the amplitude of breathing and amount of hysteresis. (b) Shows breathing amplitude as calculated from the vector length displacement of GTV centroid relative to fifth percentile reference position. One minute of data is shown here with the detected inhalation peaks indicated with red circles. (
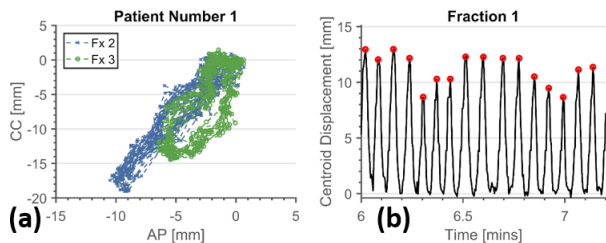


contours (a total of 1190 per fraction) was compared with the ITV generated from the entire treatment MIP (MR-ITV$_{20\,min}$).

## RESULTS

The DIR-generated contours were found to be visually acceptable in all fractions and within 7 mm, measured along the direction of maximum motion, of manually generated contours (10 frames per fraction). The motion of the GTV measured during CT- and MR-simulation is listed in Table 2 (top row, motion in red). Figure 2 shows the location of the GTV centroid for the first 500 s of two fractions for Patient 1, plotted as AP *vs* CC directions

normalized to the fifth percentile of each axis. The motion of the GTV centroid shows a distinct pattern in each fraction. Fraction 3 showed the largest motion (not shown for figure clarity), with mean GTV centroid displacement of 18.0 ± 3.0 mm (± one standard deviation). Fraction 1 shows the smallest mean centroid displacement (11.1 ± 2.0 mm) and Fraction 2 shows an increase in the amount of hysteresis. Figure 2 shows an example of 1 min of breathing data from the middle of Fraction 1 for the same patient, showing the detected inhalation peaks (red circles) overlaid on the motion amplitude (black line). Table 2 (bottom row) shows the mean (red) and standard deviation (black) of the GTV centroid motion for each fraction and patient. The agreement between the 4DCT, 172 s MR and cine mode MR data sets vary.

Figure 3 shows the intra- and interfractional variation in the displacement magnitude of the GTV centroid. Individual inhalations are shown (grey dots), with the number of inhalations (*N*) measured per fraction listed on the *x*-axis. Boxplots per fraction showing the median (black line), interquartile range (coloured boxes) and min–max range (whiskers) of the displacements are displayed over the data. The interval endpoints of the medians are displayed as notches in the boxes, representing the 95% confidence interval on the median. Figure 4 shows an example of the ITV generation (Patient 3, Fraction 1 shown, with GTV area = 12.3 mm$^2$). Figure 4 shows MIP image from a 20-min fraction of SBRT, and the corresponding ITV contour, resulting in an ITV area = 26.6 mm$^2$. Figure 4 shows the "best-case" scenario (*i.e.* closest to the entire treatment) for a MR-ITV$_{10\,s}$, generated from 10 s snapshot which includes a deep inhalation,

Figure 3. Variation in amplitude of breathing, showing amplitude of individual inhalations (grey dots) and boxplots per fraction showing the median (black line), interquartile range (coloured boxes) and min–max range (whiskers) of the amplitudes. The interval endpoints of the medians are displayed as notches in the boxes, representing the 95% confidence interval on the median.
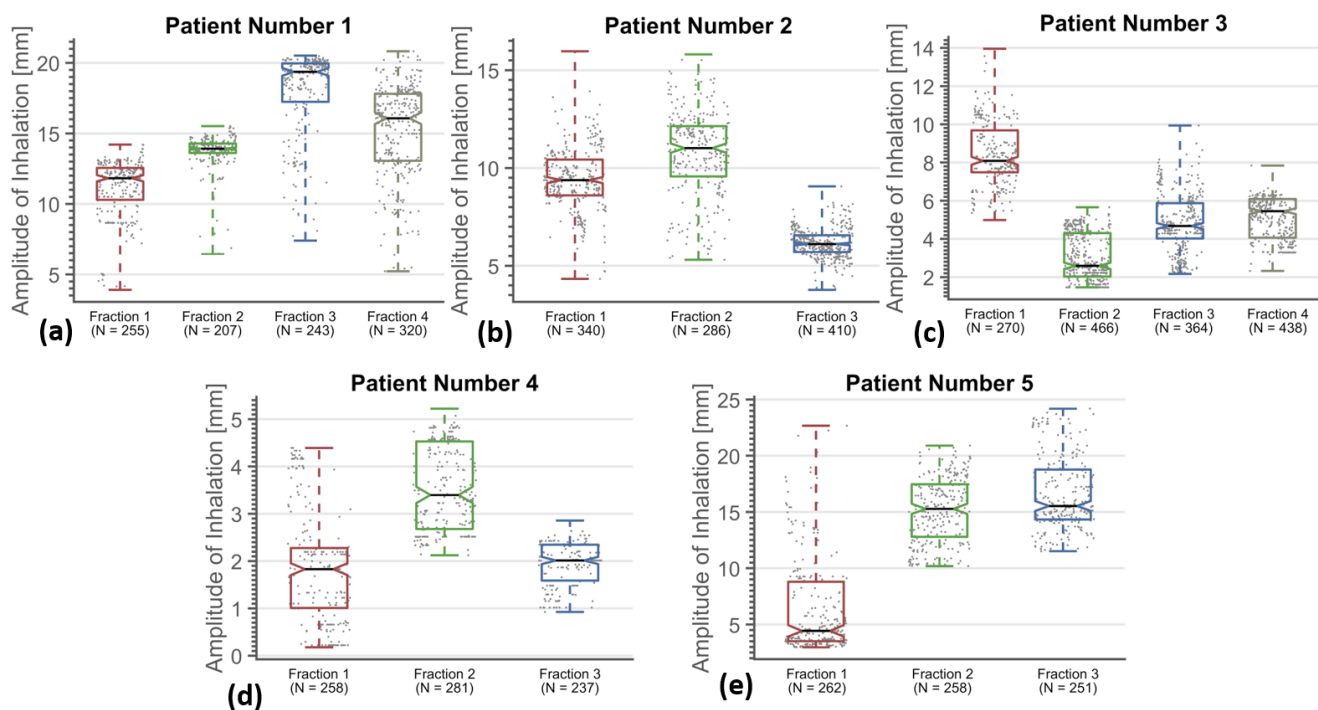
and generates an ITV with ITV area = 26.2 mm$^2$. Figure 4 shows the "worst-case" scenario, where no motion is captured during the 10 s snapshot, and the ITV is similar in size to the GTV (ITV area = 12.6 mm$^2$). ITV area was chosen as a metric, as opposed to maximum diameter, as area will reflect changes to both depth of breathing and any changes in hysteresis, as observed in Figure 2.

It is worth noting that MR-ITV$_{20\ min}$ includes all time points, and as such may be susceptible to outliers, such as involuntary patient motions (coughs etc.) which would have potentially little dosimetric consequence. Cumulative histograms showing the distribution of ITV area with respect to the entire treatment MIP for each fraction, each patient, are shown in Figure 4. MR-ITV$_{10\ s}$ with area as small as 40% of the MR-ITV$_{20\ min}$ are observed. The median (50th percentile) values range from 45 to 90%.

## DISCUSSION

This study presents analyses of a large amount of tumour tracking data, and is the first study of its kind to analyse patients in the treatment position during treatment over multiple fractions. Many of the previous studies were performed with arms-down, and all were done without the immobilization devices used for treatment being present. While many studies investigating breathing motion have studied the effect of intrafractional breathing variation, the data presented here show that interfractional variation in breathing amplitude may be larger than previously considered.

Only patients with tumours with sufficient contrast for tumour tracking on MRI were chosen for this study, which limited the size of the patient cohort. The choice of patient inclusion in the study was made by physician, based on the ability to easily identify the GTV on the simulation images. Comparison between contours drawn on different modalities is problematic, owing to inherent differences in contrast and acquisition times, especially when acquired during free breathing. The comparison between the 4DCT and MR (both the high resolution 172 s acquisition and the cine-mode data) ITV dimensions shown in Table 2 has a large amount of intrinsic uncertainty. Of note is that even with a 172 s acquisition acquired at simulation, the ITV can be smaller than that acquired during subsequent day's treatment (*e.g.* Patient 1, Fraction 3). Further work is merited to investigate if patient specific margins can be calculated from a single session of breathing data which will account for interfraction motion changes. For more advanced approaches to treatment delivery, such as tumour tracking with prediction modelling, we show here that a single 4DCT is not sufficient to estimate the variation in tumour motion throughout the course of treatment, and more robust motion modelling is warranted. While the acquisition of multiple 4DCTs[20] has the ability to offer increased information to validate the ITV, the unwanted increase in patient imaging dose typically prevents such studies.

As improvements to hardware and acquisition sequences continue to increase image quality and temporal resolution, MRI will offer more accurate measurement of breathing variability owing to its non-ionizing nature and the ability to image for an extended period of time.[21] Currently the ViewRay is the only

clinically available MR-guided system, and uses a gated approach to irradiate the tumour at a specific breathing phase.[22] These initial five patients were treated free breathing; we have since then transitioned to a breath-hold (deep inspiratory) treatment protocol with only a 3–5 mm planning target volume margin added to the GTV acquired at breathold (no ITV). Gated treatments suffer from lower efficiency; various publications suggest improved accuracy and sparing of normal tissues can be achieved by adjusting the beam delivery to track the tumour,[23–27] as well as shorter treatment times. Dynamic MRI currently has poor spatial resolution compared with 4DCT, and suffers from low lung signal intensity and magnetic susceptibility effects.[28, 29] The limitations of real-time MRI, as well as the unavoidable latencies of tracking, such as data processing time and hardware reaction time (up to 500 ms in the case of the ViewRay system)[22] suggest that motion modelling[30, 31] and breathing prediction methods[32–34] will still have an important role to play in MRI-guided treatments, as well as X-ray-guided treatments. The data presented here show that interfractional motion is an important consideration for such approaches.

One obvious limitation to this study is the small patient sample size, which limits the power to detect significant differences in breathing variation between tumours of different size and location. However, the large number of breaths and days tracked in each patient gives large statistical power to the analysis, and all five patients in the cohort demonstrated significant variation in between fractions. Similar simulations of the variability of ITV accuracy have been presented in the literature, *e.g.* Dou et al[35] have performed a statistical study of one-dimensional simulations of 4DCT tumour motion measurement error using 50 patient's external breathing surrogates. They show that 61% of patients exhibit a 5% chance of tumour motion underestimation, depending on the snapshot of breathing taken during 4DCT, but data are only presented for a single session. The data presented here represent a continuation of that approach, and although limited in the number of patients, has the advantage of tumour tracking over multiple days and not relying on surrogate data.

A proprietary free-form deformable registration (similar to the work of Lu et al[36]) is available on the ViewRay clinical treatment delivery system which allows a user specified contour to be tracked in real time, but this real time tracking data are currently not available to be exported from the system for further analysis, so was not used in this study. In addition, tracking low contrast tumours can be difficult using real time approaches owing to limited signal-to-noise in the low field images. Various approaches have been documented in the literature for improved real-time tracking, including snakes-based tracking, template matching and manifold learning,[37–41] including a recent approach using scale-invariant feature transform descriptors applied directly to ViewRay cine images.[41] As real-time tracking is not required for this study, we used an offline approach based on anatomy-based multilevel multiresolution optical flow analysis and thin-plate splines for registering the frames. Although the frame-to-frame registration is approximately 12 times slower than real time, even when running on a GPU cluster, this approach provides improved tracking of tumours that lack well-defined boundaries

in the presence of limited signal-to-noise owing to the low field strength. Target registration error was typically on the order of one voxel.

The amplitude of motion in this study is measured as the vector length of the distance between the current GTV centroid and its fifth-AP and CC percentile position. This approach effectively removes any effect of a baseline drift from the analysis. As image guidance (either CBCT for patient positioning or continual MRI for MR-guided treatments) is the clinical standard, we chose to remove the baseline shifts from the analysis in this study, and focus on the accuracy of the area of the ITV contour generated for planning. Corrective action such as patient repositioning either before or during treatment to account for a baseline shift is possible as long as the treatment is image-guided. However, replanning to account for an inaccurate ITV is not achievable without real-time adaptive treatment planning.

The dosimetric effect of under covering the true ITV is not considered here and should be investigated further. Another limitation of this study was the acquisition of 2D data, which prohibited tracking of motion in 3D. We assume here that out of plane motion is small in comparison to the sagittal plane. Fast 3D sequences to allow true 4D-MRI imaging is an active area of development, but the resultant images have poor resolution

in the axial slice direction, on the order of 10 mm,[14] often suffer from low signal-to-noise ratio, and are not yet clinically available.

A recent retrospective study to evaluate whether gated radiotherapy, whereby radiation is only delivered when the tumour is within the GTV contour, provides dosimetric improvements to organs-at-risk in lung SBRT showed that only patient's with the largest tumour motion (>2 cm) would receive a clinically relevant benefit.[42] Given the success of current ITV-based lung SBRT treatments in achieving local control without significant toxicity,[43–45] current ITV approaches may be adequate, but still leave room for improvement in cases for which minimizing treatment margins is critical. MR's improved ability to accurately delineate organs at risk, combined with gated- or tracked-delivery of lung SBRT, may lead to the expansion of SBRT to more central lung tumours owing to the associated reduction in toxicity in normal tissue.

## CONCLUSIONS

The results presented here indicate that variability of both intra- and interfractional tumour motion and variation in the amount of hysteresis should be taken into account during both motion modelling of breathing motion and planning of lung radiotherapy.

## REFERENCES

1. Zamora DA, Riegel AC, Sun X, Balter P, Starkschall G, Mawlawi O, et al. Thoracic target volume delineation using various maximum-intensity projection computed tomography image sets for radiotherapy treatment planning. *Med Phys* 2010; 37: 5811–20. doi: https://doi.org/10.1118/1.3504605

2. Underberg RW, Lagerwaard FJ, Cuijpers JP, Slotman BJ, van Sörnsen de Koste JR, Senan S. Four-dimensional CT scans for treatment planning in stereotactic radiotherapy for stage I lung cancer. *Int J Radiat Oncol Biol Phys* 2004; 60: 1283–90. doi: https://doi.org/10.1016/j.ijrobp.2004.07.665

3. Cai J, McLawhorn R, Read PW, Larner JM, Yin FF, Benedict SH, et al. Effects of breathing variation on gating window internal target volume in respiratory gated radiation therapy. *Med Phys* 2010; 37: 3927–34. doi: https://doi.org/10.1118/1.3457329

4. Cai J, Read PW, Baisden JM, Larner JM, Benedict SH, Sheng K. Estimation of error in maximal intensity projection-based internal target volume of lung tumors: a simulation and comparison study using dynamic magnetic resonance imaging. *Int J Radiat Oncol Biol Phys* 2007; 69: 895–902.

   doi: https://doi.org/10.1016/j.ijrobp.2007.07.2322

5. van Heeswijk RB, Bonanno G, Coppo S, Coristine A, Kober T, Stuber M. Motion compensation strategies in magnetic resonance imaging. *Crit Rev Biomed Eng* 2012; 40: 99–119. doi: https://doi.org/10.1615/CritRevBiomedEng.v40.i2.20

6. Cai J, Read PW, Altes TA, Molloy JA, Brookeman JR, Sheng K. Evaluation of the reproducibility of lung motion probability distribution function (PDF) using dynamic MRI. *Phys Med Biol* 2007; 52: 365: 365: 73. doi: https://doi.org/10.1088/0031-9155/52/2/004

7. Blackall JM, Ahmad S, Miquel ME, McClelland JR, Landau DB, Hawkes DJ. MRI-based measurements of respiratory motion variability and assessment of imaging strategies for radiotherapy planning. *Phys Med Biol* 2006; 51: 4147–69. doi: https://doi.org/10.1088/0031-9155/51/17/003

8. Seregni M, Paganelli C, Lee D, Greer PB, Baroni G, Keall PJ, et al. Motion prediction in MRI-guided radiotherapy based on interleaved orthogonal cine-MRI. *Phys Med Biol* 2016; 61: 872: 872: 87. doi: https://doi.org/10.1088/0031-9155/61/2/872

9. Liu Y, Yin FF, Rhee D, Cai J. Accuracy of respiratory motion measurement of 4D-MRI: a comparison between cine and sequential acquisition. *Med Phys* 2016; 43: 4938066: 4938066: . doi: https://doi.org/10.1118/1.4938066

10. Cai J, Chang Z, Wang Z, Paul Segars W, Yin FF. Four-dimensional magnetic resonance imaging (4D-MRI) using image-based respiratory surrogate: a feasibility study. *Med Phys* 2011; 38: 6384–94. doi: https://doi.org/10.1118/1.3658737

11. Cai J, Chang Z, Yin F. Imaging tumor motion using 4D-MRI. *Int J Radiat Oncol Biol Phys* 2011; 81: S122–S123. doi: https://doi.org/10.1016/j.ijrobp.2011.06.251

12. Cai J, Read PW, Larner JM, Jones DR, Benedict SH, Sheng K. Reproducibility of interfraction lung motion probability distribution function using dynamic MRI: statistical analysis. *Int J Radiat Oncol Biol Phys* 2008; 72: 1228–35. doi: https://doi.org/10.1016/j.ijrobp.2008.07.028

13. Cai J, Read PW, Sheng K. The effect of respiratory motion variability and tumor size on the accuracy of average intensity projection from four-dimensional computed tomography: an investigation based on dynamic MRI. *Med Phys* 2008;

**35**: 4974–81. doi: https://doi.org/10.1118/1.2982245

14. Koch N, Liu HH, Starkschall G, Jacobson M, Forster K, Liao Z, et al. Evaluation of internal lung motion for respiratory-gated radiotherapy using MRI: Part I-correlating internal lung motion with skin fiducial motion. *Int J Radiat Oncol Biol Phys* 2004; **60**: 1459–72. doi: https://doi.org/10.1016/j.ijrobp.2004.05.055

15. Plathow C, Fink C, Ley S, Puderbach M, Eichinger M, Zuna I, et al. Measurement of tumor diameter-dependent mobility of lung tumors by dynamic MRI. *Radiother Oncol* 2004; **73**: 349–54. doi: https://doi.org/10.1016/j.radonc.2004.07.017

16. Cai J, Read PW, Altes TA, Molloy JA, Brookeman JR, Sheng K. Evaluation of the reproducibility of lung motion probability distribution function (PDF) using dynamic MRI. *Phys Med Biol* 2007; **52**: 365–73. doi: https://doi.org/10.1088/0031-9155/52/2/004

17. Min Y, Neylon J, Shah A, Meeks S, Lee P, Kupelian P, et al. 4D-CT Lung registration using anatomy-based multi-level multi-resolution optical flow analysis and thin-plate splines. *Int J Comput Assist Radiol Surg* 2014; **9**: 875–89. doi: https://doi.org/10.1007/s11548-013-0975-7

18. White BM, Vennarini S, Lin L, Freedman G, Santhanam A, Low DA, et al. Accuracy of routine treatment planning 4-dimensional and deep-inspiration breath-hold computed tomography delineation of the left anterior descending artery in radiation therapy. *Int J Radiat Oncol Biol Phys* 2015; **91**: 825–31. doi: https://doi.org/10.1016/j.ijrobp.2014.11.036

19. Horn BKP, Schunck BG. Determining optical flow. *Artif Intell* 1981; **17**: 185–203. doi: https://doi.org/10.1016/0004-3702(81)90024-2

20. Atkins K, Varchani A, Nam TL, Fuss M, Tanyi JA. Interfraction regional variation of tumor breathing motion in lung stereotactic body radiation therapy (SBRT). *Int J Radiat Oncol Biol Phys* 2013; **87**: S68–S69. doi: https://doi.org/10.1016/j.ijrobp.2013.06.178

21. Sarma M, Hu P, Rapacchi S, Ennis D, Thomas A, Lee P, et al. Accelerating dynamic magnetic resonance imaging (MRI) for lung tumor tracking based on low-rank decomposition in the spatial-temporal domain: a feasibility study based on simulation and preliminary prospective undersampled MRI. *Int J Radiat Oncol Biol Phys* 2014; **88**: 723–31. doi: https://doi.org/10.1016/j.ijrobp.2013.11.217

22. Mutic S, Dempsey JF. The ViewRay system: magnetic resonance-guided and controlled radiotherapy. *Semin Radiat Oncol* 2014;

**24**: 196–9. doi: https://doi.org/10.1016/j.semradonc.2014.02.008

23. Keall PJ, Kini VR, Vedam SS, Mohan R. Motion adaptive x-ray therapy: a feasibility study. *Phys Med Biol* 2001; **46**: 1–10. doi: https://doi.org/10.1088/0031-9155/46/1/301

24. Keall PJ, Barton M, Crozier S.Australian MRI-Linac Program, including contributors from Ingham Institute, Illawarra Cancer Care Centre, Liverpool Hospital, Stanford University, Universities of Newcastle, Queensland, Sydney, Western Sydney, and Wollongong. The Australian magnetic resonance imaging-linac program. *Semin Radiat Oncol* 2014; **24**: 203–6. doi: https://doi.org/10.1016/j.semradonc.2014.02.015

25. Lagendijk JJ, Raaymakers BW, van Vulpen M. The magnetic resonance imaging-linac system. *Semin Radiat Oncol* 2014; **24**: 207–9. doi: https://doi.org/10.1016/j.semradonc.2014.02.009

26. Keall PJ, Joshi S, Vedam SS, Siebers JV, Kini VR, Mohan R. Four-dimensional radiotherapy planning for DMLC-based respiratory motion tracking. *Med Phys* 2005; **32**: 942–51. doi: https://doi.org/10.1118/1.1879152

27. Verellen D, Depuydt T, Gevaert T, Linthout N, Tournel K, Duchateau M, et al. Gating and tracking, 4D in thoracic tumours. *Cancer Radiother* 2010; **14**: 446–54. doi: https://doi.org/10.1016/j.canrad.2010.06.002

28. Biederer J, Hintze C, Fabel M, Dinkel J. Magnetic resonance imaging and computed tomography of respiratory mechanics. *J Magn Reson Imaging* 2010; **32**: 1388–97. doi: https://doi.org/10.1002/jmri.22386

29. Koch N, Liu HH, Olsson LE, Jackson EF. Assessment of geometrical accuracy of magnetic resonance images for radiation therapy of lung cancers. *J Appl Clin Med Phys* 2003; **4**: 352–64. doi: https://doi.org/10.1120/jacmp.v4i4.2510

30. Thomas D, Lamb J, White B, Jani S, Gaudio S, Lee P, et al. A novel fast helical 4D-CT acquisition technique to generate low-noise sorting artifact-free images at user-selected breathing phases. *Int J Radiat Oncol Biol Phys* 2014; **89**: 191–8. doi: https://doi.org/10.1016/j.ijrobp.2014.01.016

31. McClelland JR, Hawkes DJ, Schaeffter T, King AP. Respiratory motion models: a review. *Med Image Anal* 2013; **17**: 19–42. doi: https://doi.org/10.1016/j.media.2012.09.005

32. Ruan D. Kernel density estimation-based real-time prediction for respiratory motion. *Phys Med Biol* 2010; **55**: 1311–26. doi: https://doi.org/10.1088/0031-9155/55/5/004

33. Ruan D, Thomas D, Low DA. Objective function to obtain multiple representative waveforms for a novel helical CT scan

protocol. *Med Phys* 2015; **42**: 1164–9. doi: https://doi.org/10.1118/1.4906128

34. Ruan D, Fessler JA, Balter JM. Real-time prediction of respiratory motion based on local regression methods. *Phys Med Biol* 2007; **52**: 7137–52. doi: https://doi.org/10.1088/0031-9155/52/23/024

35. Dou TH, Thomas DH, O'Connell D, Bradley JD, Lamb JM, Low DA. Technical note: simulation of 4DCT tumor motion measurement errors. *Med Phys* 2015; **42**: 6084–9. doi: https://doi.org/10.1118/1.4931416

36. Lu W, Chen ML, Olivera GH, Ruchala KJ, Mackie TR, Weiguo L. Fast free-form deformable registration via calculus of variations. *Phys Med Biol* 2004; **49**: 3067: 3067: 87. doi: https://doi.org/10.1088/0031-9155/49/14/003

37. Lewis JH, Li R, Watkins WT, Lawson JD, Segars WP, Cerviño LI, et al. Markerless lung tumor tracking and trajectory reconstruction using rotational cone-beam projections: a feasibility study. *Phys Med Biol* 2010; **55**: 2505–22. doi: https://doi.org/10.1088/0031-9155/55/9/006

38. Shi X, Diwanji T, Mooney KE, Lin J, Feigenberg S, D'Souza WD, et al. Evaluation of template matching for tumor motion management with cine-MR images in lung cancer patients. *Med Phys* 2014; **41**: 052304: 052304: . doi: https://doi.org/10.1118/1.4870978

39. Yigitsoy M, Wachinger C, Navab N. Manifold learning for image-based breathing gating in MRI. In: Dawant B. M, Haynor D. R, eds. *Medical imaging 2011: image processing*. vol. 7962. Orlando, FL, USA: SPIE Medical Imaging; 2011.

40. Chen Q, Quan F, Xu J, Rubin DL. Snake model-based lymphoma segmentation for sequential CT images. *Comput Methods Programs Biomed* 2013; **111**: 366–75. doi: https://doi.org/10.1016/j.cmpb.2013.05.019

41. Mazur TR, Fischer-Valuck BW, Wang Y, Yang D, Mutic S, Li HH. SIFT-based dense pixel tracking on 0.35 T cine-MR images acquired during image-guided radiation therapy with application to gating optimization. *Med Phys* 2016; **43**: 279–93. doi: https://doi.org/10.1118/1.4938096

42. Kim J, Wu Q, Zhao B, Wen N, Ajlouni M, Movsas B, et al. To gate or not to gate - dosimetric evaluation comparing gated vs. ITV-based methodologies in stereotactic ablative body radiotherapy (SABR) treatment of lung cancer. *Radiat Oncol* 2016; **11**: 125. doi: https://doi.org/10.1186/s13014-016-0699-2

43. Shaverdian N, Tenn S, Veruttipong D, Wang J, Hegde J, Lee C, et al. The significance

of PTV dose coverage on cancer control outcomes in early stage non-small cell lung cancer patients treated with highly ablative stereotactic body radiation therapy. *Br J Radiol* 2016; **89**: 20150963. doi: https://doi.org/10.1259/bjr.20150963

44. Shaverdian N, Wang PC, Steinberg M, Lee P. The patient's perspective on stereotactic body radiation therapy (SBRT) vs. surgery for treatment of early stage non-small cell lung cancer (NSCLC). *Lung Cancer* 2015; **90**: 230–3. doi: https://doi.org/10.1016/j.lungcan.2015.07.009

45. Janssen S, Kaesmann L, Rudat V, Rades D. Stereotactic body radiotherapy (SBRT) with lower doses for selected patients with stage i non-small-cell lung cancer (NSCLC). *Lung* 2016; **194**: 291–4. doi: https://doi.org/10.1007/s00408-016-9849-4